Atmos. Chem. Phys. Discuss., 14, 11929–11960, 2014
www.atmos-chem-phys-discuss.net/14/11929/2014/
doi:10.5194/acpd-14-11929-2014

Atmospheric Chemistry and Physics Discussions

Observations of the scale-dependent turbulence and evaluation of the flux-gradient relationship for sensible heat for a closed Douglas-Fir canopy in very weak wind conditions

D. Vickers and C. Thomas

Oregon State University, College of Earth, Ocean, and Atmospheric Sciences, Corvallis, Oregon, USA

Received: 17 March 2014 – Accepted: 17 April 2014 – Published: 13 May 2014

Correspondence to: D. Vickers (vickers@coas.oregonstate.edu)

Published by Copernicus Publications on behalf of the European Geosciences Union.

Abstract

Observations of the scale-dependent turbulent fluxes and variances above, within and beneath a tall closed Douglas-Fir canopy in very weak winds are examined. The daytime subcanopy vertical velocity spectra exhibit a double-peak structure with peaks at time scales of 0.8 s and 51.2 s. A double-peak structure is also observed in the daytime subcanopy heat flux cospectra. The daytime momentum flux cospectra inside the canopy and in the subcanopy are characterized by a relatively large cross-wind component, likely due to the extremely light and variable winds, such that the definition of a mean wind direction, and subsequent partitioning of the momentum flux into along- and cross-wind components, has little physical meaning. Positive values of both momentum flux components in the subcanopy contribute to upward transfer of momentum, consistent with the observed mean wind speed profile. In the canopy at night at the smallest resolved scales, we find relatively large momentum fluxes (compared to at larger scales), and increasing vertical velocity variance with decreasing time scale, consistent with very small eddies likely generated by wake shedding from the canopy elements that transport momentum but not heat. We find unusually large values of the velocity aspect ratio within the canopy, consistent with enhanced suppression of the horizontal wind components compared to the vertical by the canopy.

The flux-gradient approach for sensible heat flux is found to be valid for the subcanopy and above-canopy layers when considered separately; however, single source approaches that ignore the canopy fail because they make the heat flux appear to be counter-gradient when in fact it is aligned with the local temperature gradient in both the subcanopy and above-canopy layers. Modeled sensible heat fluxes above dark warm closed canopies are likely underestimated using typical values of the Stanton number.

ACPD
14, 11929–11960, 2014

1 Introduction

Observational studies are important for improving our basic understanding of the turbulence mixing and turbulence transport for different forest canopy architectures in varying conditions (e.g., Baldocchi and Meyers, 1988; Meyers and Baldocchi, 1991; Raupach, 1994; Raupach et al., 1996; Vickers and Thomas, 2013, and references therein). Such studies are also important for more practical problems including mixing of scalars in the subcanopy, decoupling of the subcanopy (e.g., Staebler and Fitzjarrald, 2005; Vickers et al., 2012; Thomas et al., 2013; Vickers and Thomas, 2013), air-surface exchange processes (e.g., Goulden et al., 1996; Thomas et al., 2013), and parameterizations of the turbulent fluxes in terms of model-resolved bulk quantities, such as flux-gradient methods and Monin–Obukhov similarity theory.

The observations in this study are of special interest because they are characterized by a very dense canopy and very weak winds. The subcanopy has a reversed heat flux regime, where the heat flux is upward at night and downward during the day. The daytime momentum flux is typically upwards in the subcanopy associated with a decrease in the mean wind speed with increasing height between the subcanopy layer and the within-canopy layer. Analysis of such weak turbulence subcanopy conditions coupled with the reversed heat flux regime is often avoided in the literature.

In this study we analyze observations of the scale-dependent turbulent fluxes and variances above, within and beneath a tall closed Douglas-Fir canopy. In addition, we evaluate the standard flux-gradient approach for sensible heat to address the question of whether or not standard flux-gradient methods are appropriate for the subcanopy layer where the mean wind speed is very weak and decreases with height, and the primary source of heating and cooling is located at the top of the layer. Such evaluations are relevant to the ecosystem modeling community as their models typically use some form of the bulk–flux relationship and may or may not resolve the different layers separately.

ACPD
14, 11929–11960, 2014

2 Materials and methods

2.1 Site description

The data analyzed here were collected in a 33 year-old Douglas-Fir forest located in the coast range of western Oregon, USA (AmeriFlux site US-Fir, 44.646° N latitude, 123.551° W longitude, 310 m elevation) during the period 5 May through 24 October 2007 (Thomas et al., 2008; Thomas, 2011). The vertical structure of the vegetation canopy consists of a sparse understory composed mainly of Salal (Gaultheria shallon) with a maximum plant height of 0.8 m above ground level (a.g.l.) and the main Douglas-Fir (Pseudotsuga menziesii) crown space extending from 15 to 26 m a.g.l. The site is surrounded by moderately sloped terrain with a relatively flat saddle located approximately 600 m to the northeast of the tower. The canopy is very dense with a plant area index (PAI) of 9.4 $m^2 m^{-2}$ optically measured in 2004 (Model LAI2000, Licor, Lincoln, NE, USA). The winds and turbulence are very weak (Tables 1 and 2 and Fig. 1). The persistent weak wind above the canopy is thought to be due to topographic sheltering by the coast range with westerly winds.

2.2 Instrumentation

Eddy-covariance measurements of the fast response wind components, temperature, humidity and carbon dioxide concentration were collected using three-dimensional sonic anemometers (model CSAT3, Campbell Scientific Inc., Logan, UT) and colocated open-path infrared gas analyzers (model LI-7500, LI-COR Inc., Lincoln, NE) during the summer dry period from 5 May through 24 October 2007. The analysis uses 20 Hz time series data collected at three levels: above the canopy at 38 m a.g.l. (z/h = 1.5), at 16 m a.g.l. just above the lowest extent of the main crown space at 15 m a.g.l., and in the relatively open subcanopy at 4 m a.g.l. Slow response mean air temperature was measured using aspirated and shielded sensors (PRT) at 4, 16 and 38 m a.g.l., and soil temperature was measured with a thermocouple 2 cm beneath the surface.

ACPD
14, 11929–11960, 2014

The temperature of the top of the canopy layer was calculated from the downward looking longwave radiation measurement (CNR1, Kipp and Zonen) at 37 m a.g.l. and an emissivity of 0.99. This value of the emissivity was found to minimize the number of counter-gradient heat fluxes for the flux measured at 38 m and the temperature gradient between the top of the canopy and 38 m. This approach is justified by our high confidence that the 38 m heat flux should be aligned with the mean temperature gradient above the canopy at $z/h = 1.5$.

2.3 Analysis

Fluxes and variances are computed using block-averaging where variables are decomposed into a mean part and a turbulent part as

$$\phi = \overline{\phi} + \phi', \tag{1}$$

where the overbar denotes a suitable time average (the perturbation time scale τ) and ϕ represents the fast response wind components, temperature or specific humidity. Unlike running means and band-pass filters, block averaging satisfies Reynolds averaging. The time averaged fluxes and variances are then computed as the average of the instantaneous products of perturbations over some chosen flux averaging time scale λ. For example, the vertical turbulent flux of ϕ is $< w'\phi' >$, where the angle brackets indicate averaging over the flux averaging time scale.

Increasing the perturbation time scale allows larger scale motions to be included in the calculated flux, while decreasing it excludes larger scale motions. Increasing the flux averaging time scale reduces the random sampling error, but may in turn introduce additional non-stationarity (Vickers et al., 2009). Our primary calculations use $\tau = 10$ min and $\lambda = 30$ min; however, the sensitivity of our results for the Stanton number to the choices of τ and λ is explored below.

Due to the small observed tilt angles, and the general uncertainty in the justification for applying a tilt correction (or coordinate rotation), especially for very weak wind subcanopy data, we did not make any corrections to the fast response wind components

ACPD
14, 11929–11960, 2014

to account for a possible tilt in the sonic anemometers from true vertical. The average tilt angle calculated (but not used for any rotations) for the most frequent mean wind direction of west-northwest is less than 1° in the subcanopy and 3° above the canopy. It is not clear whether a non-zero angle indicates real time-averaged vertical motion or a tilted sensor.

Multiresolution decomposition (Howell and Mahrt, 1997; Vickers and Mahrt, 2003) is used to compute the scale-dependences of the vertical velocity variance, the heat flux, the momentum flux components and the velocity aspect ratio. Multiresolution analysis applied to time series decomposes the record into simple unweighted averages on dyadic time scales and represents the simplest possible orthogonal decomposition. Unlike Fourier analysis, multiresolution decomposition satisfies Reynolds averaging at all scales and does not assume periodicity.

The isotropy of the turbulence is examined using the velocity aspect ratio (Vickers and Mahrt, 2006) computed as

$$\mathrm{VAR} = \frac{2^{1/2}\sigma_w}{(\sigma_u^2 + \sigma_v^2)^{1/2}} \quad (2)$$

where σ denotes the standard deviation (e.g., $\sigma_w = \overline{w'w'}^{1/2}$). In the case where $\sigma_u = \sigma_v = \sigma_w$, VAR is unity and the turbulence is isotropic. Small values of VAR indicate mostly 2-dimensional motions that are likely non-turbulent.

A normalized turbulence intensity is evaluated as $\sigma_w U^{-1}$, where σ_w is the standard deviation of the vertical velocity and U is the mean wind speed. Large values of the normalized turbulence intensity can indicate important sources of turbulence other than the usual local shear generation.

2.4 Bulk fluxes

The bulk aerodynamic relationship for estimating surface fluxes is applied in almost all numerical models (e.g., the Community Land Model; Oleson et al., 2010) either directly

ACPD
14, 11929–11960, 2014

or indirectly in combination with other approaches. The bulk formulation for the heat flux is typically written as

$$H = \rho c_p < w'\theta' >= \rho c_p C_H U(\theta_o - \theta) \quad (3)$$

where H is the sensible heat flux, ρ is the air density, c_p is the specific heat at constant pressure, $< w'\theta' >$ is the kinematic heat flux, C_H is the Stanton number at height z (or the exchange coefficient for heat), U is the mean wind speed at height z, θ_o is the aerodynamic potential temperature, and θ is the potential temperature of the air at height z. The Community Land Model uses the aerodynamic resistance, which is equal to the inverse of the product of the Stanton number and the mean wind speed ($(C_H U)^{-1}$).

Using Monin–Obukhov similarity theory, the aerodynamic potential temperature θ_o is defined by vertically integrating the nondimensional potential temperature gradient from some level in the surface layer down to the roughness length for heat. However, since Monin–Obukhov similarity theory does not apply in the roughness sublayer, between the surface and the surface layer (e.g. Raupach, 1994), the computed aerodynamic temperature will be different from observed quantities, and therefore, rigorous evaluation of similarity theory is problematic (Mahrt and Vickers, 2004). Our estimates of the subcanopy C_H are made possible by substituting a measured temperature for the aerodynamic potential temperature in Eq. (3). In our case, we use the 2 cm soil temperature when evaluating the flux–gradient relationship in the subcanopy, and the radiative temperature of the top of the canopy when evaluating the flux-gradient method above the canopy.

ACPD
14, 11929–11960, 2014

3 Results

3.1 Turbulence structure

The composite scale-dependent vertical velocity variance, heat flux and momentum flux components above the canopy at 38 m a.g.l., in the lower part of the canopy at 16 m, and in the relatively open subcanopy at 4 m during the day and night are shown in Figs. 2 and 3, respectively. To avoid contamination of daytime and nighttime comparisons, the morning and evening transition periods have been excluded from these composites. The daytime heat flux is upwards at 16 and 38 m and downwards at 4 m, because the primary daytime radiative heating occurs in the tree crown where the leaf area density is greatest, and not at the ground surface. At night, the 16 m heat flux remains upward while the 38 m and 4 m level heat fluxes switch signs due to strong radiative cooling of the canopy.

A peculiar double-peak structure in the subcanopy vertical velocity spectra is found in about two-thirds of all cases during the day, but almost never at night. The double peaks are found for all wind directions. The first peak is found at 0.8 s, while the time scale of the second peak is 51.2 s (Fig. 2). The length scale associated with a time scale of 0.8 s is only about 0.4 m, using a subcanopy mean wind speed of 0.5 m s^{-1} in combination with Taylor's hypothesis, which may not be reliable in these very weak wind and weak turbulence conditions (Thomas, 2011). The peak in the vertical velocity spectra at 0.8 s may be associated with tree stem wake, although we have no direct measurements to confirm this. The lack of the double-peak structure in the vertical velocity spectra at night may be related to the weaker wind speeds at night (Tables 1 and 2) and subsequently less wake turbulence.

A double-peak structure is also observed in the daytime subcanopy heat flux cospectra (Fig. 2), where a local minimum in the negative heat flux is found for the range of time scales from 6.4 to 25.6 s. These time scales overlap with the range of time scales associated with the local minimum in the vertical velocity spectra (3.2 to 12.8 s), and it is likely that the reduced heat flux at intermediate time scales is in part due to the

ACPD
14, 11929–11960, 2014

reduced vertical mixing strength. It is also possible that there are canceling effects of upward and downward heat transport, although why such transport would be confined to these time scales is not known.

The daytime momentum flux cospectra at 16 and 4 m are characterized by a relatively large cross-wind component (Fig. 2). We speculate that this may be due to the extremely light and variable subcanopy winds, such that the definition of a mean wind direction, and subsequent partitioning of the stress into cross- and along-wind components, has little physical meaning. At 38 m above the canopy, where the mean wind speeds are still weak, but are much larger than in the subcanopy (Tables 1 and 2), our results agree with those typically found in the literature indicating that the cross-wind component of the momentum flux is small compared to the along-wind component. Positive values of both momentum flux components in the subcanopy at time scales exceeding about 10 s (Fig. 2) denote a net upward transfer of momentum at these scales, and are consistent with the observed decrease in the mean wind speed with height from 4 m to 16 m.

Inside the canopy at the 16 m level at night, we find relatively large momentum fluxes at the smallest resolved time scales, unlike at the other two observational levels (Fig. 3). We also find that the vertical velocity spectra are increasing with decreasing time scale at the smallest resolved scales at 16 m, unlike the other levels during day or night. These patterns are consistent with very small eddies generated by wake shedding from the canopy elements (e.g., Meyers and Baldocchi, 1991; Brunet et al., 1994; Dupont et al., 2012). These very small eddies apparently transport momentum but not heat.

3.2 Velocity aspect ratio

The velocity aspect ratio (Eq. 2) is smaller in the subcanopy compared to above the canopy at all time scales (Fig. 4), indicating that the subcanopy motions are more anisotropic (more horizontal) compared to those above the canopy, consistent with enhanced suppression of vertical velocity perturbations closer to the ground. Both above and below the canopy, VAR is maximum at time scales of 0.4 to 0.8 s, and de-

ACPD
14, 11929–11960, 2014

creases with increasing time scale. The scale-dependences of the above-canopy and subcanopy estimates of VAR are similar to those observed at a tall open canopy pine forest site (Vickers and Thomas, 2013). The decrease in VAR with decreasing time scale for time scales shorter than 0.4 s is likely a shortcoming of the instrumentation, possibly due to a preferred pathlength averaging in the vertical direction caused by the sensor geometry of the sonic anemometers.

The unusual scale dependence of VAR inside the canopy is consistent with the idea that the canopy inhibits horizontal fluctuations more than vertical ones, leading to large values of VAR that can even exceed unity in the long-term average (Fig. 4). At this site, the composite VAR reaches a local maximum of 1.5 at a time scale of 25.6 s. This enhanced suppression of the horizontal wind fluctuations compared to the vertical (large VAR) at a height where the tree crown is densest was qualitatively confirmed by visualizing the canopy flow using episodic releases of artificially generated buoyantly neutral fog.

3.3 Normalized turbulence intensity

The normalized turbulence intensity ($\sigma_w U^{-1}$) inside the canopy is much larger than either above or below the canopy, and increases from about 1 to 2 as the 38 m wind speed increases from 0 to 4 m s^{-1} (Fig. 5). Moving from within the canopy at 16 m to above the canopy at 38 m, the mean wind speed increases by a factor of 12 while σ_w increases by only a factor of 2. That is, the influence of the canopy on the flow is to strongly reduce the mean horizontal wind speed while only weakly reducing the vertical velocity fluctuations. The relative lack of suppression of the vertical velocity perturbations inside the canopy is consistent with the finding above using VAR, where the canopy elements act to suppress the horizontal fluctuations more than the vertical ones leading to large VAR inside the canopy. We are not aware of any reported values of the turbulence intensity that exceed those observed here inside the canopy.

ACPD
14, 11929–11960, 2014

3.4 Flux–gradient relationship in the subcanopy

The composite diurnal cycle of the subcanopy sensible heat flux over the entire experimental period ranges from about $1\,W\,m^{-2}$ at night to $-3\,W\,m^{-2}$ during the day (Fig. 6). The fluxes are very small as a result of the extremely weak turbulence due to the combination of weak winds above the canopy and a closed canopy (Fig. 1). Despite the very weak turbulence and very weak fluxes, a coherent temporal pattern is observed, where the heat flux is upward at night, because the ground surface is warmer than the canopy due to strong radiational cooling of the tree crowns, and is downward during the day, when the tree crowns are warmer than the ground surface. This diurnal cycle of the heat flux is opposite to the common textbook case where the heat flux is upward during the day and downward at night. It is rather remarkable that a consistent subcanopy heat flux pattern emerges despite the instrumental challenges of measuring such small heat fluxes characterized by large relative sampling errors associated with the shortcomings of computing eddy-covariance fluxes in very weak turbulence (Mahrt, 2010).

A scatter plot of the 4 m heat flux as a function of the product of the mean wind speed and the temperature difference is shown in Fig. 7. The slope of the linear regression line is an estimate of the Stanton number (C_H). The estimate for C_H of $1.1 \pm 0.04 \times 10^{-3}$ with $r^2 = 0.32$, is within the range of typical values reported for C_H in the literature of 1 to 5×10^{-3} (Stull, 1990). The large relative random sampling errors associated with the small fluxes contribute to the scatter in Fig. 7.

We could not find any other variable that explained significant additional variance in the 4 m heat flux, including soil temperature, soil moisture content, air temperature, wind speed or direction above or below the canopy, moisture flux, momentum flux, or the variances of vertical velocity, temperature or moisture. That is, the formulation in Eq. (3), assuming the exchange coefficient is known, appears to be the best formulation of the heat flux, thus confirming the flux-gradient approach for the subcanopy.

ACPD
14, 11929–11960, 2014

In addition to general agreement with previously reported C_H estimates, it is encouraging that the intercept of the regression is zero for all practical purposes (Fig. 7), which indicates that on average, and despite the large scatter, the heat fluxes are aligned with the direction of the local temperature gradient as required by the flux–gradient relationship. The zero intercept was found using the 2 cm soil temperature and the 4 m shielded and aspirated air temperature to specify the temperature difference. The zero intercept suggests that the 2 cm soil temperature measurement is representative of the average ground surface (skin) temperature in the subcanopy eddy-covariance flux footprint.

The dependence of the strength of the regression relationship, or the fraction of variance explained (r^2), and the slope (C_H) on the flux perturbation time scale and the flux averaging time scale is briefly discussed here. Neither r^2 or C_H are strongly sensitive to λ. The variance explained by the regression (r^2) increases slightly with increasing λ due to a decrease in the random sampling error. The change in C_H with flux averaging time scale is small, decreasing only 6 % for a change in λ from 30 min to 2 h. The r^2 decreases slightly with increasing τ because increasing τ increases the possibility that larger-scale, non-turbulent submesoscale motions, which may not be related to the local mean wind speed or temperature gradient, will be included in the calculated flux, especially in stable conditions (e.g., Smedman, 1988; Vickers and Mahrt, 2006; Mahrt, 2009). C_H increases with increasing perturbation time scale τ because of the systematic flux loss when using too small a value for τ to calculate the heat flux. For example, if there is significant heat flux associated with turbulent transport on time scales of 300 s and the flux is calculated using τ equal to 100 s, then the computed flux will be an underestimation for the given wind speed and temperature gradient.

An alternative approach for estimating C_H is to compute individual 30 min average estimates, equal to the heat flux divided by the product of the mean wind speed and the temperature difference (Eq. 3). The frequency distribution of such estimates is shown in Fig. 8. This approach to estimate C_H yields a mean value of 1.1×10^{-3} with a standard deviation of 2.05×10^{-3}. When computing individual 30 min average estimates of C_H,

ACPD
14, 11929–11960, 2014

we exclude cases where the product of the absolute value of the 30 min mean wind speed and the temperature difference is less than 0.1 C m s^{-1}. This is necessary to avoid dividing by a very small number or zero when solving Eq. (3) for C_H for individual 30 min periods. About 15 % of the C_H estimates are less than zero, indicating counter-gradient heat transfer (Denmead and Bradley, 1985), or more likely, very small mean fluxes and large random flux sampling errors. The negative values of C_H are associated with stronger wind speed periods.

Some of the variation in the subcanopy C_H (Fig. 8) appears to be due to variation in stability (not shown). However, we avoid plotting C_H as a function of z/L, where L is the Obukhov length scale, to eliminate the problems associated with self-correlation, where the same quantity (in this case the heat flux) is contained within two different variables (C_H and z/L) being compared to each other (Hicks, 1978; Klipp and Mahrt, 2004; Baas et al., 2006). We also avoid comparing C_H to a bulk Richardson number because both contain the temperature gradient. Values of the subcanopy stability are small compared to above the canopy.

3.5 Flux–gradient relationship above the canopy

Above the canopy, C_H is computed using a temperature difference equal to the canopy radiative temperature minus the 38 m air temperature. With such a temperature gradient defined, our estimate of C_H above the canopy using the regression slope method is $73.5 \pm 1.3 \times 10^{-3}$ (Fig. 9). This is about 65 times larger than the estimate found for the subcanopy of $1.1 \pm 0.04 \times 10^{-3}$, using 90 % confidence intervals for the slope. The linear regression explains 77 % of the variance of the heat flux at 38 m compared to 32 % of the variance at 4 m.

Stability appears to have a significant influence on the 38 m C_H leading to a bi-modal frequency distribution (Fig. 10). Stability is more important above the canopy compared to in the subcanopy in part because the daytime heat fluxes at 38 m are typically one-hundred times larger than those in the subcanopy. The mean daytime above canopy C_H

ACPD
14, 11929–11960, 2014

is $84.2 \pm 55.6 \times 10^{-3}$, while the mean nighttime above canopy C_H is $15.3 \pm 26.4 \times 10^{-3}$. Again, direct comparisons between C_H and z/L or the bulk Richardson number are avoided here to eliminate contamination of the relationships by self-correlation.

One possibility to explain the larger C_H above the canopy is that the larger surface area associated with the large leaf area density leads to more efficient transfer of heat for a given mean temperature difference and wind speed, and thus a larger exchange coefficient. Another possibility is simply that the turbulence is much stronger above the canopy. However, this difference in turbulence strength should be at least partially accounted for already in the bulk formula through the dependence on the mean wind speed, because U is proportional to the shear generation of turbulence and thus the vertical velocity fluctuations. While the larger normalized turbulence intensity above the canopy (0.32) compared to in the subcanopy (0.19) could account for some of the difference in C_H, it seems unlikely it could account for all of it.

3.6 Single source flux-gradient

Here we estimate C_H at 38 m using a single source approach where the temperature difference used to estimate the heat flux at 38 m a.g.l. is computed as the 2 cm soil temperature minus the potential temperature of the air at 38 m a.g.l. That is, the single source approach ignores the presence of the canopy, as in some model parameterizations.

Using the single source approach, C_H is negative ($-12.8 \pm 27.9 \times 10^{-3}$), suggesting that the heat fluxes are counter-gradient (Fig. 11). That is, the single source approach fails because it makes the heat flux appear to be counter-gradient when in fact the heat flux is aligned with the local temperature gradient in both the subcanopy and above-canopy layers when the two layers are considered separately.

ACPD
14, 11929–11960, 2014

4 Summary and conclusions

The daytime subcanopy heat flux is downwards because the strong radiational warming takes place in the high leaf area density of the canopy layer, not at the ground. Conversely, the nighttime subcanopy heat flux is upwards because the strong radiational cooling takes place in the canopy layer, not at the ground. A peculiar double-peak structure at time scales of 0.8 s and 51.2 s is typically observed in the subcanopy vertical velocity spectra during the day, but almost never at night. The first peak, roughly corresponding to a length scale of only about 0.4 m, may be associated with tree stem wake. The lack of a double-peak at night may be due to the weaker wind speeds at night. A double-peak structure is also observed in the daytime subcanopy heat flux cospectra. The time scales identified suggest that the reduced heat flux at intermediate time scales from 6.4 to 25.6 s is likely due to the reduced vertical mixing strength.

The daytime momentum flux cospectra inside the canopy and in the subcanopy are characterized by a relatively large cross-wind component, likely due to the extremely light and variable winds, such that the definition of a mean wind direction, and subsequent partitioning of the momentum flux into along- and cross-wind components, has little physical meaning. Positive values of both momentum flux components in the subcanopy denote an upward transfer of momentum, consistent with the observed decrease in the mean wind speed with height between the subcanopy and canopy layers. Unlike in the subcanopy or above the canopy, inside the canopy at night at the smallest resolved scales we find relatively large momentum fluxes and increasing vertical velocity variance with decreasing time scale. These patterns are likely associated with very small eddies generated by wake shedding from the canopy elements that transport momentum but not heat.

The closed canopy appears to inhibit horizontal motions more than vertical motions, leading to large values of the velocity aspect ratio and the normalized turbulence intensity in the canopy. The suppression of the horizontal wind component compared to the vertical component was qualitatively confirmed by visualizing the flow using releases of

ACPD
14, 11929–11960, 2014

buoyantly neutral fog. The subcanopy motions are more anisotropic compared to those above the canopy, consistent with enhanced suppression of vertical velocity perturbations closer to the ground.

The slope derived from linear regression of the subcanopy heat flux as a function of the product of the mean wind speed and the temperature difference yields an estimate for the subcanopy Stanton number (exchange coefficient for heat) of $1.1 \pm 0.04 \times 10^{-3}$ (90 % confidence interval for the slope). The intercept of the regression is zero, indicating that on average, and despite the large scatter, the subcanopy heat fluxes are aligned with the local temperature gradient. An alternative approach for estimating C_H, where we compute individual 30 min average estimates and average them, yields an estimate for the mean subcanopy Stanton number of 1.1×10^{-3} with a standard deviation of 2.05×10^{-3}.

The exchange coefficient for heat above the canopy is $73.5 \pm 1.3 \times 10^{-3}$, or about 65 times larger than the estimate found for the subcanopy. Stability appears to have an important influence. The mean daytime (unstable) above canopy C_H is $84.2 \pm 55.6 \times 10^{-3}$, while the mean nighttime (stable) above canopy C_H is $15.3 \pm 26.4 \times 10^{-3}$. A likely explanation for the larger C_H above the canopy compared to in the subcanopy is that the higher leaf area density in the canopy leads to more efficient transfer of heat compared to the ground surface for a given wind speed and temperature difference, and thus a larger exchange coefficient. Much stronger turbulence at 38 m may also be a factor, although this effect would seem to be already accounted for in the bulk formula through the dependence on mean wind speed and the stratification.

A single source approach for the 38 m heat flux, which uses the 2 cm soil temperature and the potential temperature above the canopy to define the temperature difference in the flux-gradient method, fails because it neglects the presence of the canopy. Such failure is likely dependent on the canopy closure and vertical structure. Neglecting the canopy at our site makes the heat flux appear to be counter-gradient when in fact it is aligned with the local temperature gradient when the two layers are considered

ACPD
14, 11929–11960, 2014

separately. This indicates that land-flux models that do not explicitly resolve the canopy and subcanopy layers may compute erroneous heat fluxes.

Acknowledgements. We gratefully acknowledge Kent Davis and Matt Trappe for field work. This research was supported by the US Department of Energy (DOE), Office of Science (BER), contract DE-FG02-06ER64318. CKT also acknowledges support from the National Science Foundation, Physical and Dynamic Meteorology, NSF Career grant AGS0955444.

References

Baas, P., Steeneveld, G. J., Van De Wiel, B. J. H., and Holtslag, A. A. M.: Exploring self-correlation in flux–gradient relationships for stably stratified conditions, J. Atmos. Sci., 63, 3045–3054, 2006. 11941

Baldocchi, D. D. and Meyers, T. P.: A spectral and lag-correlation analysis of turbulence in a deciduous forest canopy, Bound.-Lay. Meteorol., 45, 31–58, 1988. 11931

Brunet, Y., Finnigan, J., and Raupach, M. R.: A wind tunnel study of air flow in waving wheat: single-point velocity statistics, Bound.-Lay. Meteorol., 70, 95–132, 1994. 11937

Denmead, O. T. and Bradley, E. F.: Flux-gradient relationships in a forest canopy, in: The Forest-Atmosphere Interaction, edited by: Hutchison, B. A. and Hicks, B. B., D. Reidel Publ. Comp., Dordrecht, Boston, London, 421–442, 1985.

Dupont, S., Irvine, M. R., Bonnefond, J., Lamaud, E., and Brunet, Y.: Turbulent structures in a pine forest with a deep and sparse trunk space: stand and edge regions, Bound.-Lay. Meteorol., 143, 309–336, 2012. 11937

Goulden, M. L., Munger, J. W., Fan, S. M., Daube, B. C., and Wofsy, S. C.: Measurements of carbon sequestration by long-term eddy covariance: methods and a critical evaluation of accuracy, Glob. Change Biol., 2, 169–182, 1996. 11931

Hicks, B. B.: Some limitations of dimensional analysis and power laws, Bound.-Lay. Meteorol., 14, 567–569, 1978. 11941

Howell, J. and Mahrt, L.: Multiresolution flux decomposition, Bound.-Lay. Meteorol., 83, 117–137, 1997. 11934

Klipp, C. L. and Mahrt, L.: Flux–gradient relationship, self-correlation and intermittency in the stable boundary layer, Q. J. Roy. Meteor. Soc., 130, 2087–2104, 2004. 11941

ACPD
14, 11929–11960, 2014

Mahrt, L.: Characteristics of submeso winds in the stable boundary layer, Bound.-Lay. Meteorol., 130, 1–14, 2009. 11940
Mahrt, L.: Computing turbulent fluxes near the surface: needed improvements, Agr. Forest Meteorol., 150, 501–509, 2010. 11939
Mahrt, L. and Vickers, D.: Bulk formulation of the surface heat flux, Bound.-Lay. Meteorol., 110, 357–379, 2004. 11935
Meyers, T. P. and Baldocchi, D. D.: The budgets of turbulent kinetic energy and Reynolds stress within and above a deciduous forest, Agr. Forest Meteorol., 53, 207–222, 1991. 11931, 11937
Oleson, K. W., Lawrence, D. M., Bonan, G. B., Flanner, M. G., Kluzek, E., Lawrence, P. J., Levis, S., Swenson, S. C., Thornton, P. E., Dai, A., Decker, M., Dickinson, R., Feddema, J., Heald, C. L., Hoffman, F., Lamarque, J., Mahowald, N., Niu, G., Qian, T., Randerson, J., Running, S., Sakaguchi, K., Slater, A., Stockli, R., Wang, A., Yang, Z., Zeng, X., and Zeng, X.: Technical Description of version 4.0 of the Community Land Model (CLM). NCAR Technical Note $NCAR/TN-478+STR$, National Center for Atmospheric Research, Boulder, CO, 257 pp., 2010. 11934
Raupach, M. R.: Simplified expressions for vegetation roughness length and zero-plane displacement as functions of canopy height and area index, Bound.-Lay. Meteorol., 71, 211–216, 1994. 11931, 11935
Raupach, M. R., Finnigan, J., and Brunet, Y.: Coherent eddies and turbulence in vegetation canopies: the mixing-layer analogy, Bound.-Lay. Meteorol., 78, 351–382, 1996. 11931
Smedman, A. S.: Observations of multi-level turbulence structure in a very stable atmospheric boundary layer, Bound.-Lay. Meteorol., 44, 231–253, 1988. 11940
Staebler, R. M. and Fitzjarrald, D. R.: Measuring canopy structure and the kinematics of subcanopy flow in two forests, J. Appl. Meteorol., 44, 1161–1179, 2005. 11931
Stull, R. B.: An Introduction to Boundary Layer Meteorology, Kluwer Academic Publishers, Boston, 666 pp., 1990. 11939
Thomas, C. K., Martin, J. G., Law, B. E., and Davis, K. J.: Toward biologically meaningful net carbon exchange estimates for tall, dense canopies: multi-level eddy covariance observations and canopy coupling regimes in a mature Douglas-fir forest in Oregon, Agr. Forest Meteorol., 173, 14–27, doi:10.1016/j.agrformet.2013.01.001, 2013. 11931
Thomas, C. K.: Variability of subcanopy flow, temperature, and horizontal advection in moderately complex terrain, Bound.-Lay. Meteorol., 139, 61–81, 2011.

ACPD
14, 11929–11960, 2014

Thomas, C. K., Martin, J. G., Goeckede, M., Siqueira, M. B., Foken, T., Law, B. E., Loescher, H. W., and Katul, G.: Estimating daytime subcanopy respiration from conditional sampling methods applied to multi-scalar high frequency turbulence time series, Agr. Forest Meteorol., 148, 1210–1229, 2008. 11932

Vickers, D. and Mahrt, L.: The cospectral gap and turbulent flux calculations, J. Atmos. Ocean. Tech., 20, 660–672, 2003. 11934

Vickers, D. and Mahrt, L.: A solution for flux contamination by mesoscale motions with very weak turbulence, Bound.-Lay. Meteorol., 118, 431–447, 2006. 11934, 11940

Vickers, D. and Thomas, C. K.: Some aspects of the turbulence kinetic energy and fluxes above and beneath a tall open pine forest canopy, Agr. Forest Meteorol., 181, 143–151, 2013. 11931, 11938

Vickers, D., Thomas, C. K., and Law, B.: Random and systematic CO2 flux sampling errors for tower measurements over forests in the convective boundary layer, Agr. Forest Meteorol., 149, 73–83, 2009. 11933

Vickers, D., Irvine, J., Martin, J. G., and Law, B. E.: Nocturnal subcanopy flow regimes and missing carbon dioxide, Agr. Forest Meteorol., 152, 101–108, 2012. 11931

ACPD
14, 11929–11960, 2014

Table 1. Daytime averages of the wind speed (U, $\mathrm{m\,s^{-1}}$), vertical velocity variance ($< w'w' >$, $\mathrm{m^2\,s^{-2}}$), kinematic heat flux ($< w'\theta' >$, $\mathrm{K\,m\,s^{-1}}$), along-wind momentum flux component ($< w'u' >$, $\mathrm{m^2\,s^{-2}}$), and the cross-wind momentum flux component ($< w'v' >$, $\mathrm{m^2\,s^{-2}}$) at 38 m a.g.l. (above-canopy), 16 m (inside the canopy) and 4 m (subcanopy).

z (m)	U	$< w'w' >$	$< w'\theta' >$	$< w'u' >$	$< w'v' >$
38	2.3	0.59	0.20	−0.36	0.0030
16	0.19	0.13	0.0076	−0.0064	0.0081
4	0.56	0.014	−0.0024	0.0043	0.0077

ACPD
14, 11929–11960, 2014

Table 2. Same as Table 1 except for nighttime averages.

z (m)	U	$< w'w' >$	$< w'T' >$	$< w'u' >$	$< w'v' >$
38	0.94	0.085	−0.0049	−0.046	−0.0067
16	0.14	0.020	0.0074	−0.00034	0.0021
4	0.29	0.0054	0.0015	0.00023	−0.00029

ACPD
14, 11929–11960, 2014

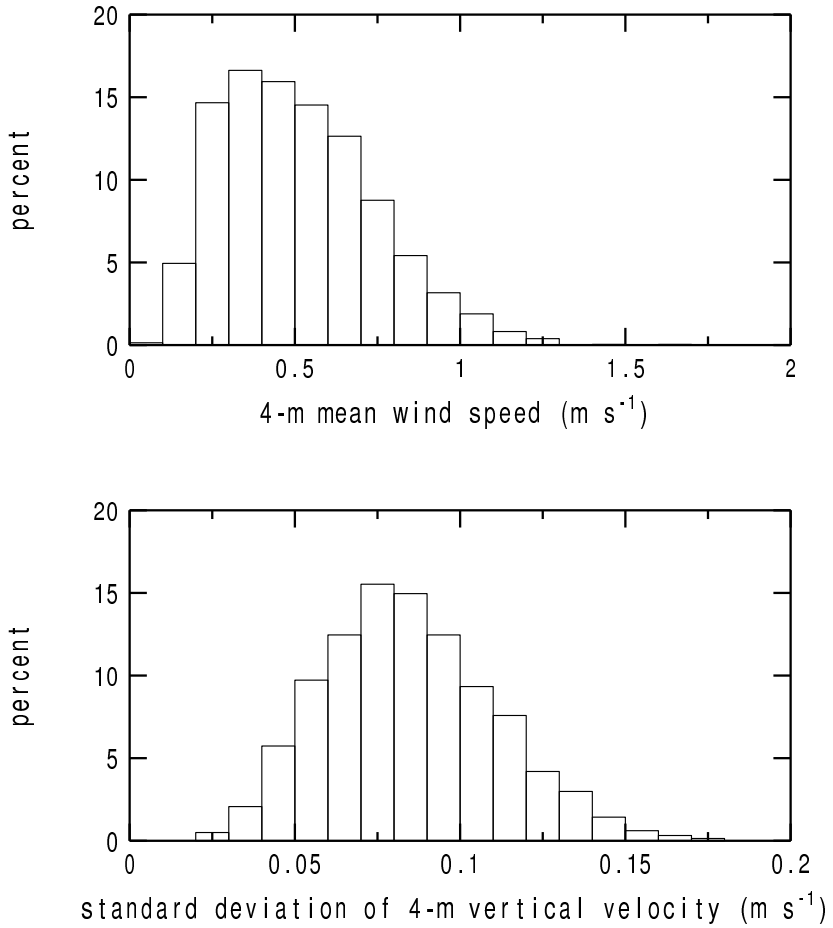

Fig. 1. The frequency distribution of the subcanopy mean wind speed (top) and the standard deviation of vertical velocity (bottom).

ACPD
14, 11929–11960, 2014

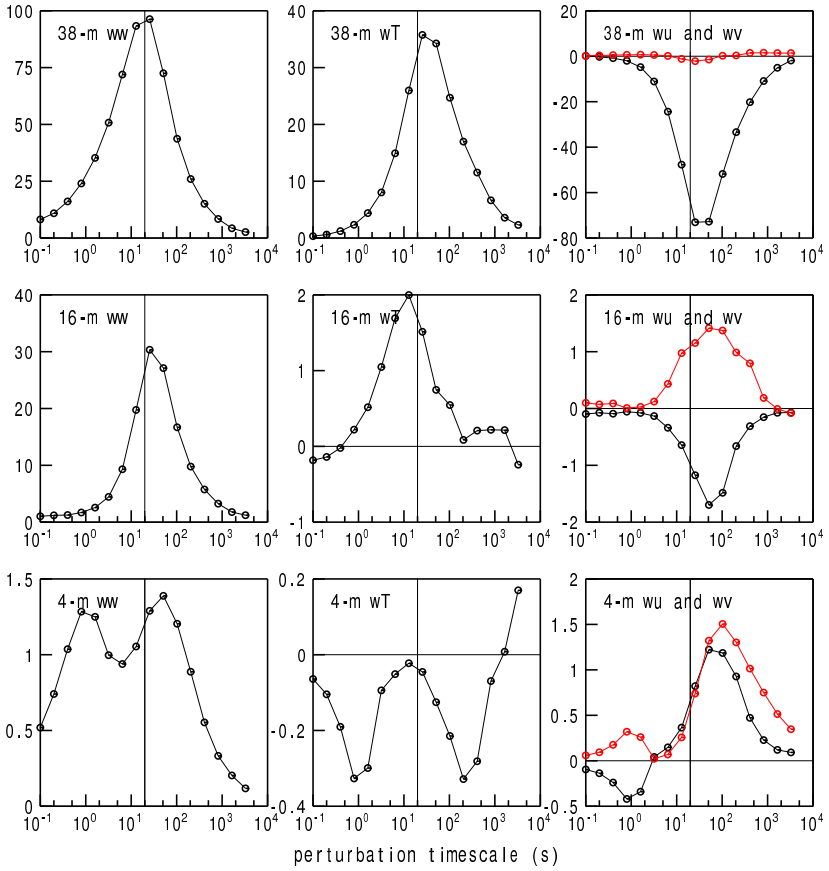

Fig. 2. Composites of three levels of daytime vertical velocity spectra ww ($m^2 s^{-2}$, left column), kinematic heat flux cospectra wT ($K m s^{-1}$, middle column), and the along- and cross-wind (red) components of the momentum flux (wu and wv) ($m^2 s^{-2}$, right column). All quantities have been multiplied by one-thousand. The vertical line in each panel denotes $\tau = 20$ s.

ACPD
14, 11929–11960, 2014

Turbulence in very weak wind conditions

D. Vickers and C. Thomas

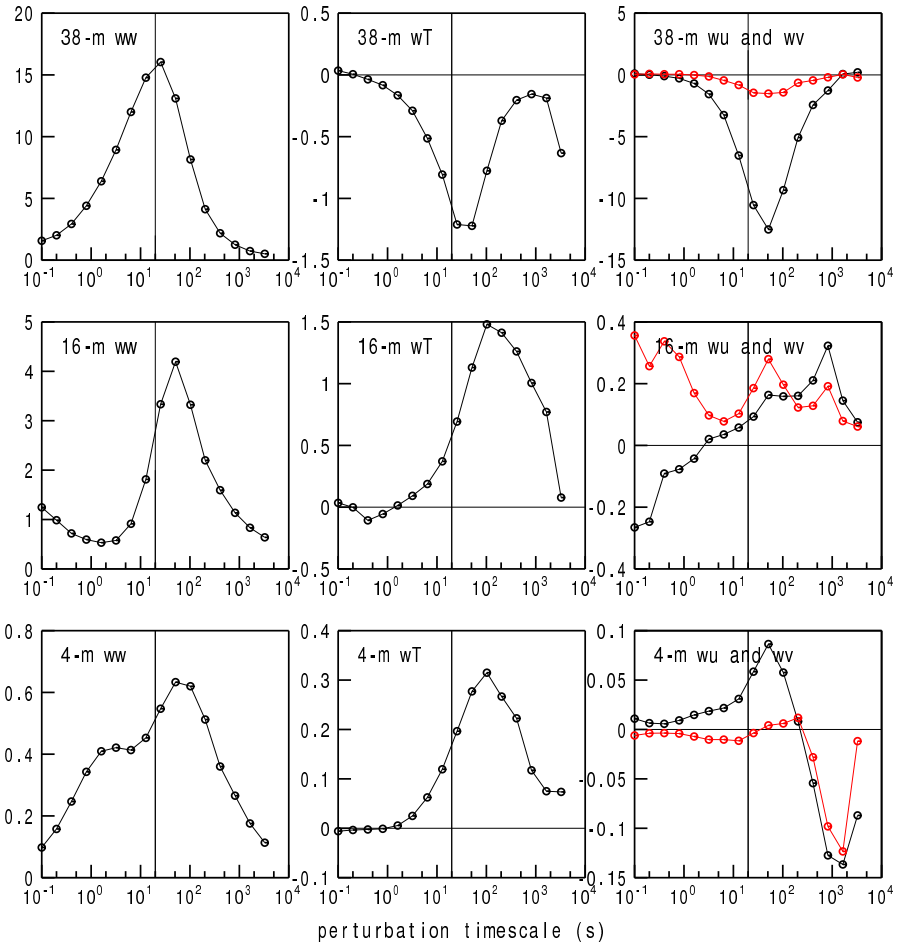

Fig. 3. Same as Fig. 2 except for nighttime.

ACPD
14, 11929–11960, 2014

Turbulence in very weak wind conditions

D. Vickers and C. Thomas

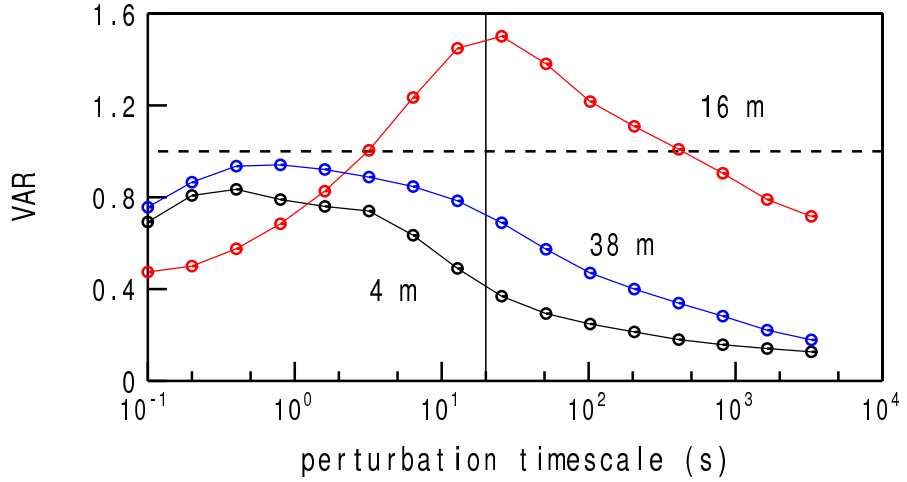

Fig. 4. Three levels of the scale-dependence of the velocity aspect ratio VAR. The vertical line denotes $\tau = 20$ s. The horizontal dashed line represents unity.

ACPD
14, 11929–11960, 2014

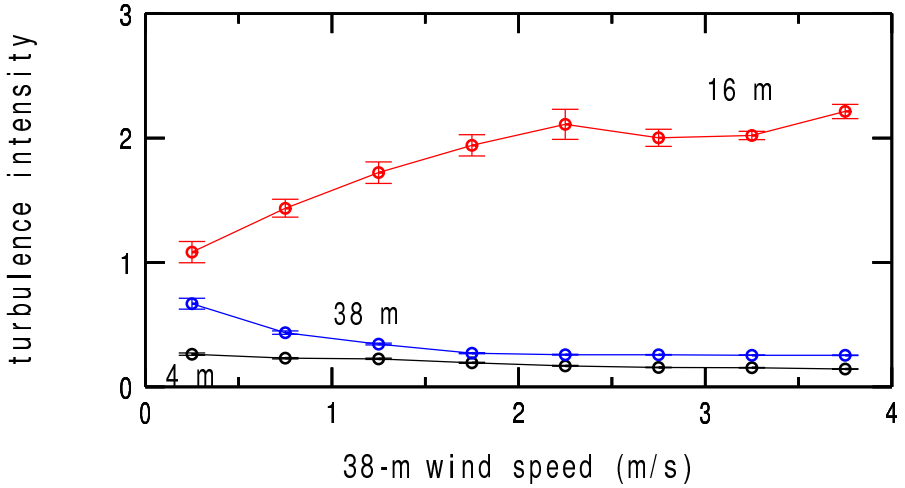

Fig. 5. The normalized turbulence intensity at three levels as a function of the wind speed above the canopy. Error bars denote ± one standard error.

ACPD
14, 11929–11960, 2014

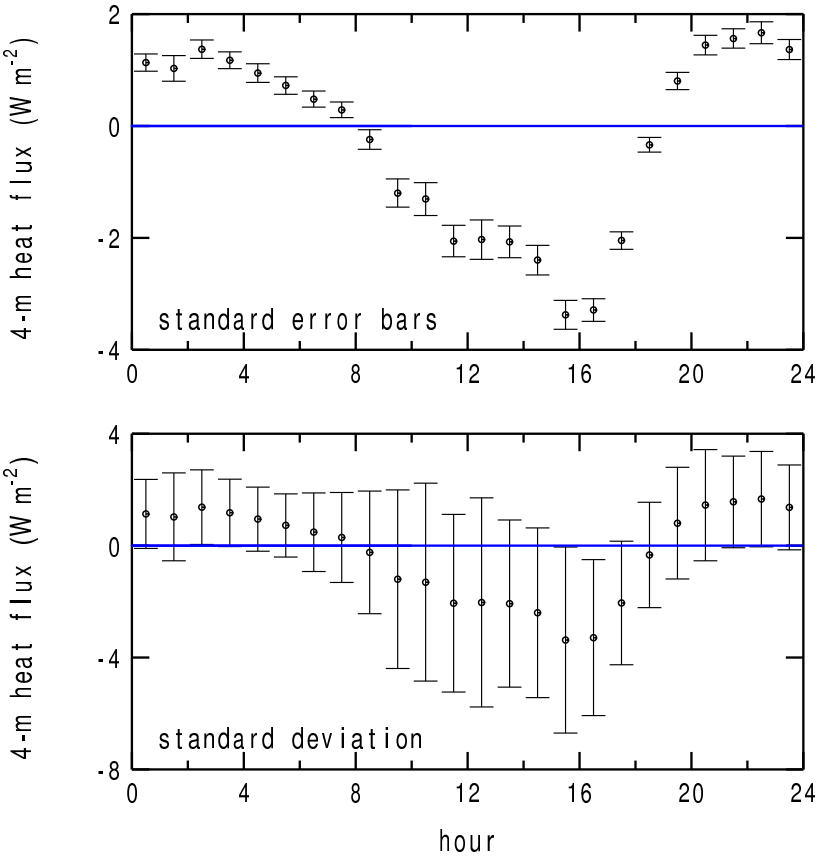

Fig. 6. The observed diurnal cycle of the subcanopy sensible heat flux with standard error bars (top) and ± one standard deviation (bottom), where the uncertainty is due to the day-to-day variability in the heat flux for a given hour of the day over the entire 5 month period.

ACPD
14, 11929–11960, 2014

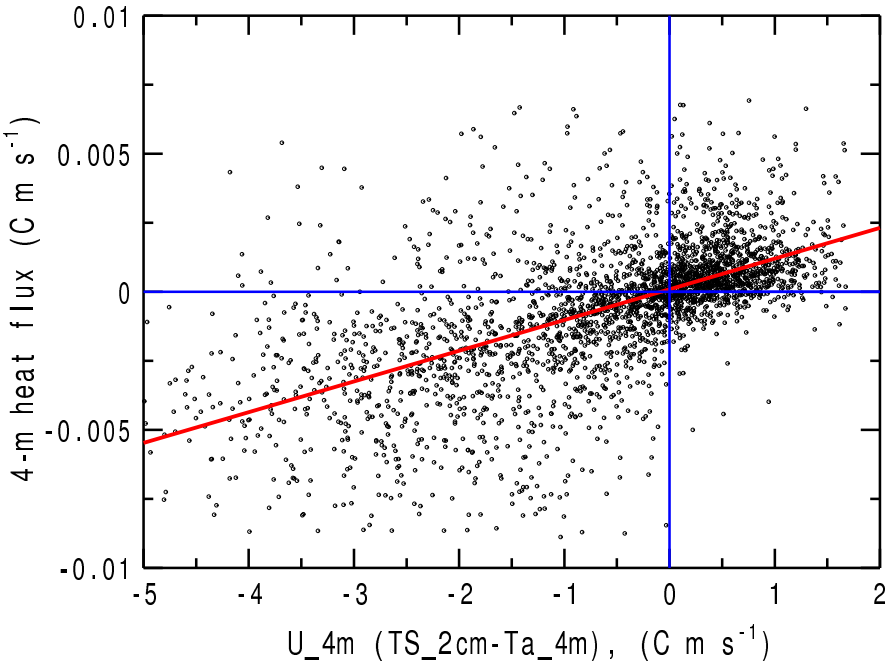

Fig. 7. A scatter plot of the 30 min average subcanopy kinematic heat flux as a function of the product of the mean wind speed and the temperature difference. The slope of the linear regression line (red) is an estimate of the subcanopy Stanton number (C_H). The estimate for C_H using this approach is $1.1 \pm 0.04 \times 10^{-3}$, using a 90 % confidence interval for the slope. The regression explains 32 % of the variance.

ACPD
14, 11929–11960, 2014

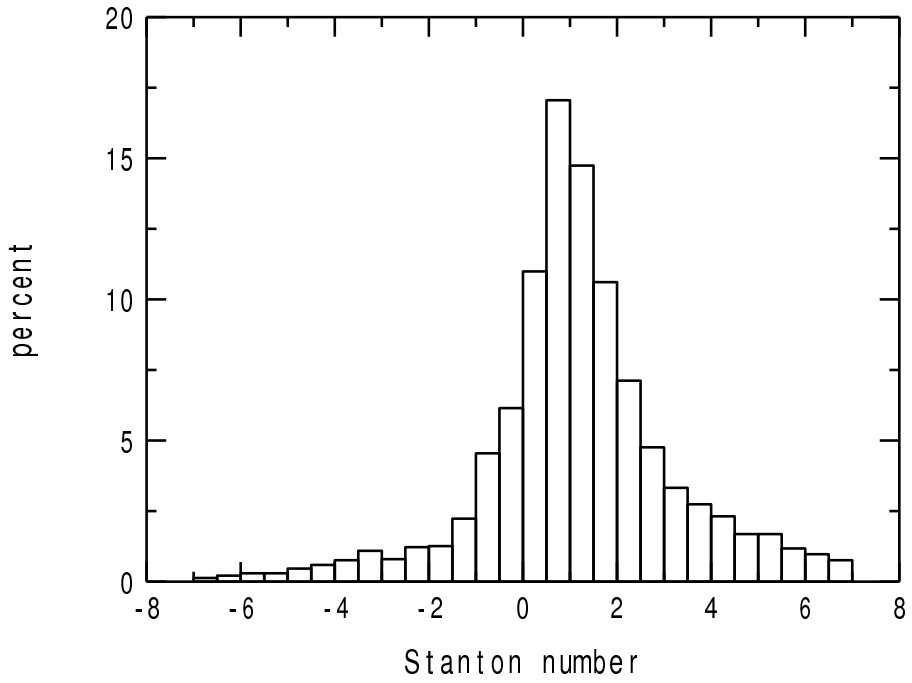

Fig. 8. The frequency distribution of the subcanopy Stanton number (multiplied by one-thousand) where each 30 min estimate is computed as the heat flux divided by the product of the mean wind speed and the temperature difference. This approach for estimating the Stanton number yields a mean value of 1.1×10^{-3} and a standard deviation of 2.05×10^{-3}.

ACPD
14, 11929–11960, 2014

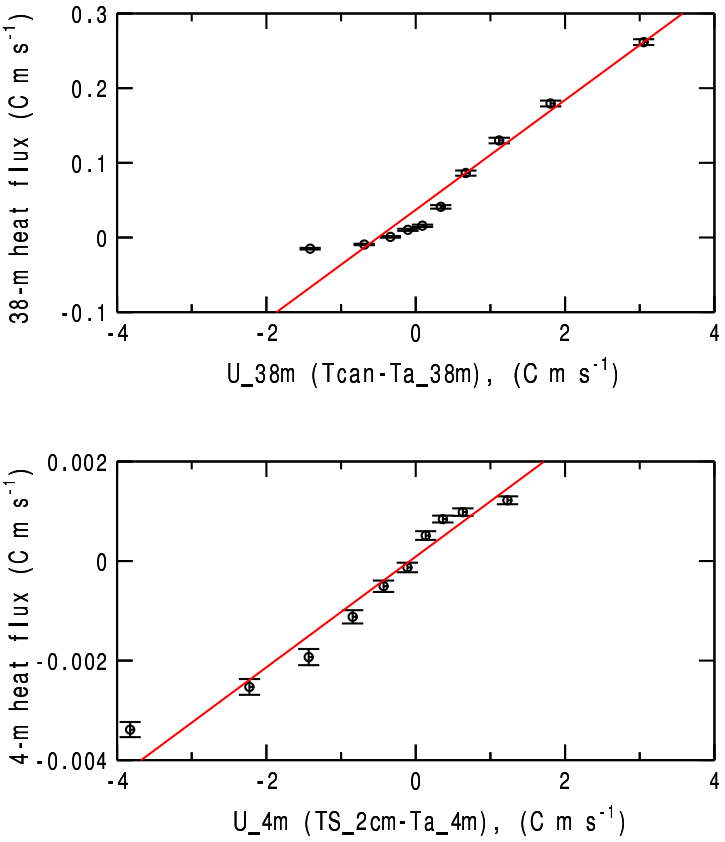

Fig. 9. The kinematic heat flux as a function of the product of the mean wind speed and the temperature difference at 38 m (top panel) and at 4 m (bottom). The slopes of the linear regression lines (red) are estimates of the Stanton number: $73.5 \pm 1.3 \times 10^{-3}$ at 38 m, and $1.1 \pm 0.04 \times 10^{-3}$ at 4 m. Each of the ten class averages contains an equal number (282) of 30 min samples. Error bars denote ± one standard error.

ACPD
14, 11929–11960, 2014

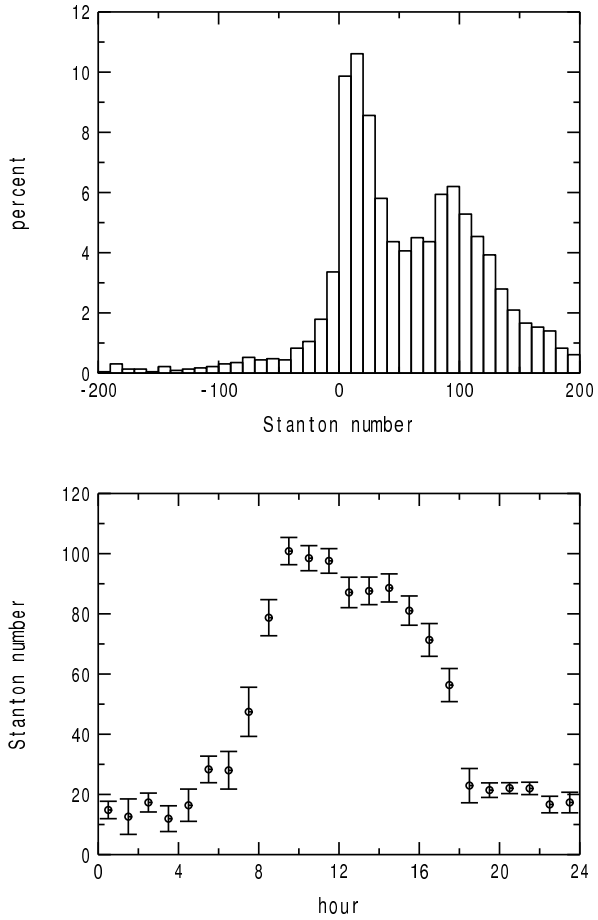

Fig. 10. The frequency distribution (top panel) and the diurnal cycle (bottom) of the above canopy Stanton number multiplied by one-thousand. Error bars denote ± one standard error.

ACPD
14, 11929–11960, 2014

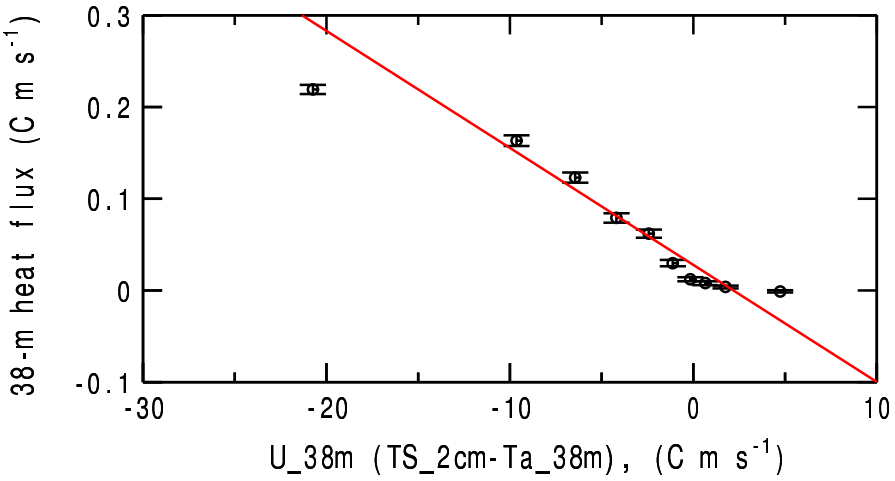

Fig. 11. The kinematic heat flux as a function of the product of the mean wind speed and the temperature difference using the single source approach (see text). The slope of the linear regression line (red) is estimate of the Stanton number: $-12.8 \pm 27.9 \times 10^{-3}$. Each of the ten class averages contains an equal number (282) of 30 min samples. Error bars denote ± one standard error.

ACPD
14, 11929–11960, 2014